Configuration and Control Strategies for Maneuvering Supersonic Flight

Kevin P. O'Brien[1]
and
Timothy T. Takahashi[2]
Arizona State University, Tempe, Arizona, 85287

The Bell X-2, the first aircraft to reach Mach 3, had severe stability and control problems at high-speeds. In this paper, we discuss three potential solutions to help solve its lateral-directional stability problems: traditional Aileron-Rudder Interconnect (ARI), using differential tail for roll control, and increasing its vertical tail area. We use stability and control screening parameters developed during the 1970s and 1980s for transonic combat to help determine if the X-2 could have been saved. From the ARI analysis, we determined that for the traditional ARI, the X-2 would require ~10% interconnect at altitudes lower than 50,000- ft with the interconnect gain increasing all the way up to ~30% for altitudes up to 70,000 ft. The use of differential tail for roll, common on transonic fighters, was unhelpful because the existing horizontal was not big enough; the aircraft would have less than 1-deg sideslip trim capability before the controls saturate. Enlarged vertical tail area greatly improved the lateral-directional stability; this recovered favorable $C_n\beta\ dynamic$ and $LCDP$ values throughout a good portion of the flight envelope. In general, an enlarged vertical tail appears to be the best solution in recovering the lateral-directional stability.

Nomenclature

a	=	local speed of sound, ft/s
α	=	angle of attack, deg
ALT	=	altitude, ft
b	=	span, ft
β	=	sideslip angle
$\bar{c}$	=	reference chord ("Mean Geometric Chord") length, ft
C_D	=	coefficient of drag
C_L	=	coefficient of lift
C_l	=	rolling moment coefficient (CRM)
C_{lr}	=	rolling damping due to yaw rate
C_{lp}	=	rolling damping due to roll rate
C_m	=	pitching moment coefficient (CPM)
C_{mq}	=	pitch damping due to pitch rate
C_n	=	yawing moment coefficient (CYM)
C_{nr}	=	yaw damping due to yaw rate
C_{np}	=	yaw damping due to roll rate
C_Y	=	side force coefficient
$dC_l/dail$	=	rolling moment due to aileron
$dC_l/d\beta$	=	rolling moment due to sideslip ("Dihedral Effect")
$dC_l/drud$	=	rolling moment due to rudder
$dC_n/dail$	=	yawing moment due to aileron
$dC_n/d\beta$	=	yawing moment due to sideslip
$dC_n/drud$	=	yawing moment due to rudder
$dC_y/d\beta$	=	side force due to sideslip
delev	=	elevator deflection,
Ixx	=	rolling moment of inertia, slug-ft^2
Iyy	=	pitching moment of inertia, slug-ft^2
Izz	=	yawing moment of inertia, slug-ft^2
KEAS	=	knots equivalent airspeed, knots
KTAS	=	knots true airspeed, knots
LCDP	=	lateral control departure parameter
M	=	Mach Number
m	=	aircraft mass, lbm
n, n_z	=	load factor

[1] M.S. Candidate – Aerospace Engineering, School for the Engineering of Matter, Transport and Energy, Arizona State University, Tempe, AZ. AIAA Student Member
[2] Professor of Practice – Aerospace Engineering, School for the Engineering of Matter, Transport and Energy, Arizona State University, Tempe, AZ. AIAA Associate Fellow.

p	=	roll rate, rad/s
φ/β	=	stick fixed yaw to roll stability ratio
$\bar{q}$	=	dynamic pressure, lbf-ft^2
q	=	pitch rate, rad/s
r	=	yaw rate, rad/s
S_{ref}	=	reference area, ft^2
τ_r	=	Roll Mode Time Constant
τ_s	=	Spiral Mode Time Constant
ω_{SP}	=	Short Period frequency, Hz.
ω_{DR}	=	Dutch Roll frequency, Hz.
ζ_{SP}	=	Short Period damping
ζ_{DR}	=	Dutch Roll damping

I. Introduction

BELL AVIATION developed the X-2 under a cooperative research program with the National Advisory Committee for Aeronautics (NACA), the United States Air Force, and the United States Navy. Development began in July of 1947 with a contract to build a total of two aircraft just a few months before Chuck Yeager broke the sound barrier in the Bell X-1.[1] The main research goals that X-2 was designed to study were high-speed flight (M > 2), high-altitude flight, and aerodynamic heating.

FIGURE 1 – BELL X-2 and its Boeing B-50 Mothership

A significant difference between the previous X-1 and the X-2 (see FIGUREs 1 and 2) was its swept-wing planform. Wing sweep is a key parameter in high-speed flight as it helps control shock wave formation and its associated byproducts. By sweeping the wing, the airfoils maintain a subsonic leading edge (and hence reduce shock-induced separation and maintain leading-edge-suction) at supersonic flight speeds. Another key feature of the X-2 was its all-moving horizontal tail; it gives the X-2 configuration increased pitch control power at supersonic speeds. [2]

FIGURE 2 – BELL X-1

While the X-2 program had many setbacks and complications, the program eventually broke a number of records. On September 9th, 1956, Iven Kincheloe set an altitude record of 126,200-ft.[1] On September 27th, 1956, Mel Apt reached Mach 3.2 but, ultimately died in tragedy with the loss of the aircraft. [1] During the flight, Apt experienced a series of unstable modes resulting in him ejecting his escape capsule from the aircraft. [1] He was unable to get out of the capsule and died when it struck the ground. [1]

Since Bell designed the X-2 just after World War II, it predated the existence of small and powerful digital computers. Today, combat aircraft have onboard digital computers to augment flight control. During the 1940s and early 1950s, engineers had access to "analog computers" to simulate flight; the few digital computers in existence could only solve simple problems at a massive time expense. While analog computers could simulate the motion of an aircraft in real time, they were not particularly effective to support mission planning outside of tested flight regimes. FIGURE 3 shows the analog simulator, which involved a pilot sitting in a room full of electronics moving a "stick" to keep a dot on a cathode-ray-tube centered. [2] The X-2 program used the Goodyear Electronic Digital Analyzer (GEDA). [3] The data for the GEDA came from limited theoretical knowledge, flight test, and wind tunnel models. Given the lack of computational power at the time, the X-2 did not have a flight computer onboard.

FIGURE 3 - NASA Test Pilot Steve Ishmael at the stick of X-2 GEDA five-deg of freedom analog simulator [3]

The main focus of this paper is to discuss a variety of key stability and control screening parameters, developed during the 1960s, 1970s, and 1980s, and look back retrospectively to see how these could be used to improve the top-level design or detailed design of the X-2. Should engineers fundamentally modify the aerodynamic configuration of the X-2 to make it safe to maneuver at high supersonic speeds? Alternatively, could the existing X-2 aerodynamic configuration be "saved" if a more modern computer could have been installed to implement Mach and α dependent control mixing schemes such as aileron-rudder interconnects (ARI) or used differential tail rather than differential aileron to command roll?

II. Basic Lateral-Directional Stability Issues

In our previous paper, 'An Investigation of the Bell X-2 and the Factors that Led to its Fatal Accident', we examined the final flight of the X-2 and the factors that led to its crash in more detail. [2] In that analysis, we discussed stability details such as inertial coupling, adverse yaw, and supersonic spin susceptibility. [2] We found that the proximate cause of the fatal accident was due to a risk-taking management strategy in flight operations **and** the inherently unstable characteristics of the X-2. The X-2 suffered greatly from adverse yaw over a wide range of Mach numbers. Without a primary yaw controller at high Mach numbers, the adverse yaw was uncorrectable. Consequently, it would depart from stable flight after any major pilot roll inputs. We summarize its stability problems in the following paragraphs.

The major differences in aircraft flight dynamics between subsonic and high-speed aircraft stem from differences in geometry and fundamental mass properties. This is especially true with rocket-powered aircraft as they cannot store the required fuel within the wing. A conventional low-speed aircraft carries significant payload (and/or stores and engines) along its wings; this feature results in a large fraction of vehicle mass being positioned far from the body centerline. Many high-speed aircraft have clean, thin wings; fuel, stores, and engines are not spread out along the span but concentrated along the centerline. This fundamental change results in the mass moments of inertia of conventional and high-speed aircraft being quite different. Thus, when $I_{yy} \gg I_{xx}$ the aircraft is often referred to as being body heavy whereas if $I_{yy} \ll I_{xx}$ then the aircraft is wing heavy. [4] These changes in the mass moments of inertia then lead to the increased likelihood of Inertia Coupling.

A. Inertia Coupling

These interesting mass properties eventually led to the discovery of Inertia Coupling. Inertia Coupling is a phenomenon where a disturbance in one axis of the aircraft is also felt about another. This problem began to appear in multiple experimental high-speed aircraft and thus became an area of high interest, resulting in many later X-planes studying this phenomenon. Inertia Coupling becomes present once the aircraft reaches a critical frequency; the Dutch Roll motions can "cross-talk" into the Short Period pitching mode. [2] At this point, resonance occurs, and the aircraft is subjected to uncontrollable motion about all its axes. [3] Similarly, when coupling of the Roll and Spiral Modes occurs it is referred to as Lateral Phugoid Coupling. One suggested way to screen for Inertia Coupling is by looking at the principal mass moments of inertia. The Primary Coupling Ratio given by Eq. 1 can suggest the tendency for the aircraft to experience Inertia Coupling. [3]

$$\frac{I_{xx} - I_{yy}}{I_{zz}} \tag{1}$$

As this ratio becomes more negative and approaches -1, it suggests that there is a higher tendency for the aircraft to experience Inertia Coupling. Day reports some numerical values for Inertia Coupling prone aircraft; see TABLE 1. [3] We note that for typical passenger aircraft, this parameter is closer to zero and/or positive as I_{xx} is typically close to or larger than I_{yy}.

TABLE 1

Aircraft	Primary Coupling Ratio
X-15	-0.94
X-3	-0.88
Space Shuttle	-0.84
YF-102	-0.81
F-100A	-0.71
X-2	-0.70

B. Pitch Disturbances Arising from Yaw Disturbances Triggered by the Adverse Yaw from Ailerons

As we stated previously, one of the X-2's most prevalent problems was uncorrectable adverse yaw. [2]

When the ailerons are deflected, adverse yaw occurs due to differences in drag resulting in a yawing moment. This yawing moment may help self-coordinate a turn; this is called proverse yaw. If the induced yawing moment is destabilizing it is called adverse yaw. Pilots (or autopilots) must correct significant adverse yaw, if left uncorrected adverse yaw drives the vehicle to substantial sideslip angles. The lateral-directional stability of most aircraft declines precipitously beyond a critical sideslip angle, where the vertical tail begins to stall.

FIGURE 4 illustrates how excessive adverse yaw led to the X-2 simultaneously experiencing both a lateral-directional and longitudinal departure. [1] The adverse yaw of the X-2 was sufficient that a sharp roll command at high speeds led to the formation of a high-sideslip angle. That high-sideslip angle, interacting with the static dihedral effect of the airframe ($dCl/d\beta$<<0) caused a lagging opposite rolling motion. Through Inertia Coupling, the energy in this nascent oscillation is also cross-coupled into pitch disturbances.

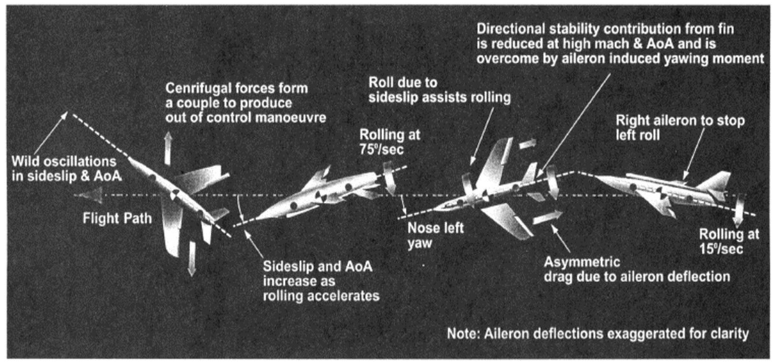

FIGURE 4- Inertia Coupling / Adverse Yaw Coupling of Bell X-2 [1]

C. Control Mixing Schemes to Reduce Adverse Yaw

Engineers can limit adverse yaw using either simple or complex control blending schemes. An example of this blending may occur with non-collective aileron deflections (i.e., one aileron deflects up more than the other deflects down) as well as through coordinated rudder inputs. Very complex generalized blending schemes where each and every movable surface is independently scheduled are beyond the focus of this paper; note the Bell X-2 has only 5 aerodynamic control surfaces: an aileron on each wing, an elevator panel on each horizontal tail fin, and a single panel rudder. Here, we consider the effects of a simple aileron-rudder interconnect (ARI). An ARI will treat the "aileron" as an antisymmetric collective deflection of the wing-mounted surfaces and the "rudder" as a deflection of the hinged surface on the vertical tail. The goal of the ARI is to utilize the primary yaw controller, here the physical rudder, to trim the induced yawing moment to zero.

D. Total Flight Envelope Approach to Flight Dynamics Analysis

Moving forward, more analysis has been focused on describing how the aircraft's stability varies with speed and altitude. This capture of the flight envelope is shown using "Sky Maps". In these plots, the speed or angle of attack is set to the *x*-axis and the altitude to *the y*-axis. The parameter of interest is then plotted as a contour plot to show the trends along an operating envelope. This will allow the designer to see how the stability of the aircraft varies with independent variables like Mach and altitude, but also key flight parameters variables such as angle of attack or dynamic pressure. An example of a Sky Map is shown in FIGURE 5. This is our preferred format to display various stability and control screening parameters.

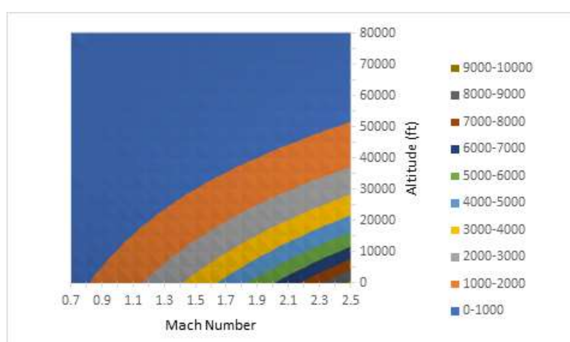

FIGURE 5 – Example of Sky Map showing Dynamic Pressure Variation

E. Need to Address Stick Fixed Aerodynamic Damping

As this project has continued, we incorporated additional stability and control screening parameters into our analysis. These parameters seem to have a substantial effect on the aircraft and thus should be checked for any high-speed aircraft design.

As aircraft fly faster and faster another area of concern now is the damping of key rigid body frequencies. As an aircraft's speed begins to approach the high supersonic and especially hypersonic speeds, the damping of the Short Period and Dutch Roll modes begin to fall off toward zero. [5] This is of major concern; without damping, these oscillatory modes will begin to have a strenuous effect on the pilot and lead to departure from stable flight. This will result in the eventual need for synthetic damping through a closed-loop control system.

F. Investigate Tendency to Spiral-Roll Couple

Another area of concern that we will address is the possibility of Roll-Spiral mode coupling. This coupling results in the aircraft experiencing a "Lateral Phugoid" coupling. This occurs when the Roll and Spiral modes begin to sit on one another and thus can "crosstalk" with one another. [6] [7] In this further development of a screening tool, we now consider the Roll and Spiral mode time constants. The coupling of the Roll and Spiral modes can cause departure from stable flight through modes such as supersonic spin.

G. Set Lower Bound to Cnβdynamic

When looking back at lateral directional stability, Takahashi, Griffin & Grandhi propose an updated version of the Weissman chart, shown in FIGURE 7 on pg. 7. [6] The bounds on Weissman's original chart were heavily based on the few aircraft studied at the time. This results in some of the region bounds being questionable. In 1978, Skow proposed a revision to the A-Region bound on $C_n\beta\ dynamic$. [8] This shifts the minimal acceptable *Cnβdynamic* bound from zero to: $Cn_\beta\ Dynamic > 0.004$. Takahashi, Griffin & Grandhi concur; they believe the new bound seems to greatly improve confidence in the handling qualities of an aircraft as some aircraft that boarder the "A"→ "F" region are either okay or completely depart. With the "A" region moved over, the aircraft is much more departure resistant. We discuss more details on the Weissman chart in Section V.

III. Mathematics to Assess Handling Qualities Flaws

As we completed more research regarding the history of aircraft stability & control and handling quality screening metrics, we became aware of a concise set of characterizing parameters that need to be considered. These consist of: 1) documenting the "open-loop" frequency and damping of the aerodynamic rigid body modes, 2) documenting the trim limits of the airframe, and 3) understanding the effects of deflecting control surfaces on basic stability. Most of the screening parameters rely upon linearized approximations; they are easy for today's engineers to assess during preliminary design.

To begin the detailed stability and control analysis, for each Mach and altitude pair the flight lift coefficient is calculated assuming lift equal weight at some load factor. From this, the corresponding flight angle of attack can be calculated along with the pitching moment curve slope and the lift curve slope. Equation 2 gives the Short Period frequency in rad/sec and Equation 3 is used to calculate the pitch responsiveness. [4] For physical insight, recall that 6.28 rad/sec is approximately 1-Hz.

$$\omega_{SP_{rad/sec}} = \sqrt{\frac{\left(-57.3\left(\frac{dCm}{d\alpha}\right) * q * S_{ref} * \bar{c}\right)}{I_{yy}}} \tag{2}$$

$$\frac{n}{\alpha} = \frac{\left(57.3 * q * S_{ref} * \left(\frac{dCL}{d\alpha}\right)\right)}{W} \tag{3}$$

To approximate the Short Period damping, Yechout [5], gives Eqs. 4 through 6.

$$M_q = \frac{Cm_q \bar{q} S_{ref} \bar{c}^2}{2 I_{yy} VKTAS \left(\frac{6076}{3600}\right)} \tag{4}$$

$$\frac{Z_a}{U_1} \approx \frac{\bar{q} S_{ref}}{m * VKTAS \left(\frac{6076}{3600}\right)} \left(57.3 * \frac{dC_L}{d\alpha}\right) \tag{5}$$

$$\xi_{sp} \approx -\frac{\left(M_q + \frac{Z_\alpha}{U_1}\right)}{2\omega_{sp}} \tag{6}$$

To determine how these parameters affect the handling and control qualities of the aircraft, we use MIL 8785-C. [9] While this handbook/standard is not a cookbook, it does give the designer a general idea for what a good aircraft should feel like. MIL 8785-C suggests that the pitch responsiveness (gee's per incidence) and stick fixed Short Period frequency (ω_{sp}) are important criteria to evaluate longitudinal handling qualities; see FIGURE 6.

In MIL 8785-C, [9] there are three charts broken up for the following phases of flight: Category A which "requires rapid maneuvering, precision tracking or precise flightpath control"; Category B- is "accomplished using gradual maneuvers and without precision tracking, although accurate flight-path control may be required"; Category C- is "accomplished during gradual maneuvers and usually require accurate flight-path control." Each chart is broken up into three levels describing the pilot workload: LEVEL 1 is described as having good flying qualities suitable for the mission phase; LEVEL 2 is described as having flying quality characteristics that require more workload out of the pilot which degrades mission performance; LEVEL 3 indicates that the aircraft is still safe to operate however, the pilot workload is far too much for the mission to be completed effectively. The aircraft is dangerous to fly if operated outside LEVEL 3 boundaries. These charts were converted into equations, for use in determining the longitudinal stability and handling qualities of the aircraft.

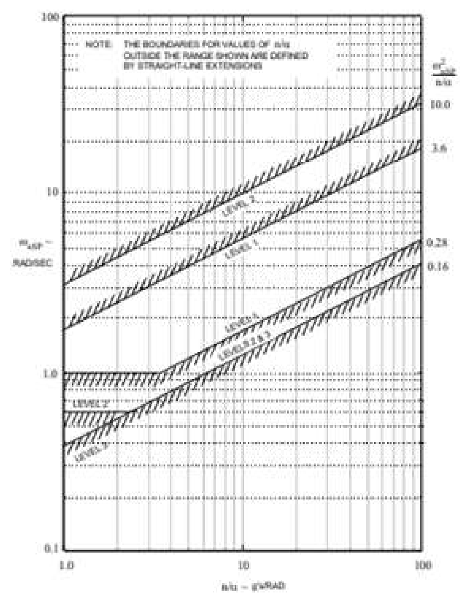

FIGURE 6 - MIL STD 8785C Category A chart [9]

When looking at lateral-directional stability there a many screening parameters of interest. This is due to the lateral-directional stability being the most tender and the source of most catastrophic departures. One key parameter of interest is $C_n\beta\ dynamic$. This parameter is proportional to the square root of the Dutch Roll frequency; if it is negative as that will cause the frequency to be indeterminate (i.e. the oscillatory mode to be unstable). The other major parameter of interest is called the Lateral Control Departure Parameter (*LCDP*). *LCDP* measures the coupling between the roll and yaw effects of the primary roll controller and the inherent lateral and directional stability of an airframe. [10] We can compute $C_n\beta\ dynamic$ and *LCDP* for each point of interest on a given flight using equations 7 and 8:

$$C_n\beta\ dynamic = \left(\frac{dCn_{Body}}{d\beta}\right) * \cos(\alpha) - \left(\frac{dCl_{Body}}{d\beta}\right) * \left(\frac{I_{zz}}{I_{xx}}\right) * \sin(\alpha) \tag{7}$$

$$LCDP = \frac{dCn_{Body}}{d\beta} - \frac{dCl_{Body}}{d\beta} * \frac{\left(\frac{dCn_{Body}}{d\ aileron}\right)}{\left(\frac{dCl_{Body}}{d\ aileron}\right)} \tag{8}$$

To determine if the aircraft is prone to control coupling, the Bihrle-Weissman chart (as shown below in FIGURE 7) is commonly used. [11] [12] [13] By plotting $LCDP$ and $C_n\beta\ dynamic$, general lateral-directional stability characteristics can be obtained. “The A region indicates that the aircraft is highly departure and spin resistant showing that the aircraft is very stable. The B region indicates that the aircraft is still spin resistant but can be subjected to roll reversals inducing departure. The C region indicates a weak spin resistance and a strong roll reversal resulting in departure. The D region indicates both strong spin tendencies and roll reversal resulting in departure. The E region is characterized as having weak spin tendency, moderate departure, and roll reversals, affected by secondary factors. The F region has weak departure and spin resistance, no roll reversal, heavily influenced by secondary factors. Lastly, the U region has high directional instability.” [11] Takahashi, Griffin and Grandhi suggest an updated version of the chart following Skow criterion; see FIGURE 7. [8] This updated figure removes a large chunk of upper A-F region where the X-2 stability was as shown in our previous paper. [2]

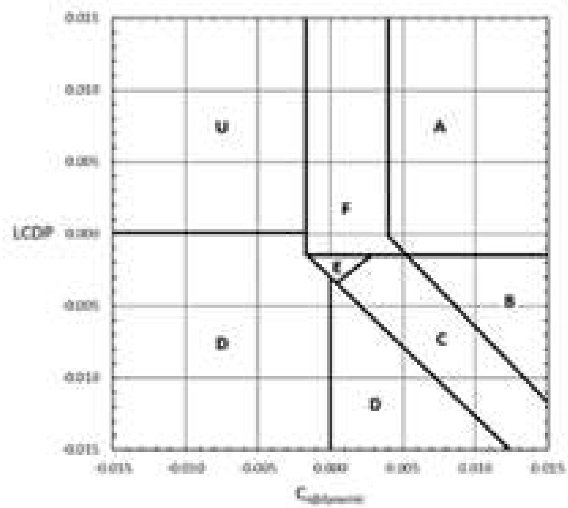

FIGURE 7 – Evolved-Bihrle-Weissman Chart after Takahashi, Griffin & Grandhi [6]

The unaugmented, stick fixed Dutch Roll frequency is estimated using $C_n\beta\ dynamic$ as: [4]

$$\omega_{DR\_HZ} = \frac{1}{2\pi} * \sqrt{\frac{\left(57.3 * C_n\beta\ dynamic * q * S_{ref} * b\right)}{I_{zz}}} \tag{9}$$

The Dutch Roll damping is estimated using Eqs. 10-12. [5]

$$N_r = \frac{Cn_r\bar{q}S_{ref}b^2}{2I_{zz}VKTAS\left(\frac{6076}{3600}\right)} \tag{10}$$

$$\frac{Y_\beta}{U} \approx \frac{\bar{q}S_{ref}}{m * VKTAS\left(\frac{6076}{3600}\right)}\left(57.3\frac{dCY}{d\beta}\right) \tag{11}$$

$$\xi_{DR} \approx -\frac{\left(N_r + \frac{Y_\beta}{U}\right)}{2\omega_{DR}} \tag{12}$$

To check for Spiral-Roll mode coupling both the Roll mode time constant and Spiral mode time constant are now calculated. The Roll mode is estimated using Eqs. 13 and 14. [5]

$$L_P = C_{l_p}\frac{\bar{q}S_{ref}b^2}{2I_{xx}VKTAS\left(\frac{6076}{3600}\right)} \tag{13}$$

$$\tau_R \approx -\frac{1}{L_p} \tag{14}$$

The Spiral Mode while a bit more involved is calculated using Eqs. 15-20. [5]

$$L_\beta = 57.3\frac{dC_l}{d_\beta}\frac{\bar{q}S_{ref}b}{I_{xx}} \tag{15}$$

$$N_\beta = 57.3 \frac{dC_n}{d_\beta} \frac{\bar{q} S_{ref} b}{I_{zz}} \tag{16}$$

$$L_r = Cl_r \frac{\bar{q} S_{ref} b^2}{2 I_{xx} VKTAS \left(\frac{6076}{3600}\right)} \tag{17}$$

$$N_r = Cn_r \frac{\bar{q} S_{ref} b^2}{2 I_{zz} VKTAS \left(\frac{6076}{3600}\right)} \tag{18}$$

$$s \approx \frac{L_\beta N_r - N_\beta L_r}{L_\beta + N_\beta \left(\frac{I_{xz}}{I_{xx}}\right)} \tag{19}$$

$$\tau_s \approx -\frac{1}{s} \tag{20}$$

The last area that needs attention is the problem of adverse yaw, a "closed loop" variation of LCDP can be computed based on a "feed-forward" aileron-rudder interconnect (ARI). Handling qualities can be improved if adverse yaw can be neutralized; $LCDP \sim \frac{dCn_{Body}}{d\beta}$ in the absence of aileron adverse yaw. To eliminate adverse yaw, the ARI must be scheduled on a Mach Number and angle of attack basis. A simple ARI can be defined as the ratio of the yawing moment of the primary roll control over the primary yaw controller shown in Eq. 22.

$$0 = CYM_{aileron} - C_1 * CYM_{rudder} \tag{21}$$

$$ARI(\%) = \frac{CYM_{aileron}}{CYM_{rudder}} \tag{22}$$

One thing that also must be considered is the effectiveness of the primary yaw device. On the Bell X-2, engineers deemed the rudder ineffective at high-speeds and thus it was mechanically locked at supersonic speeds; this renders ARI impossible. Our VORLAX models indicate that the rudder has some effect at these speeds, so it could be used in a powered-flight-control ARI system. If differential elevator is used as a roll effector, then the process of creating an ARI is slightly more complicated with a second round of interpolation being required.

IV. General Comments on High-Speed Vehicle Configurations

The Bell X-2 was conceived at a time when high-speed aerodynamics were not well understood. Consequently, its control surface configuration closely resembles that of a conventional subsonic aircraft. To get an idea of how high-speed aircraft design has evolved over the years, we will examine the control surface layout of a variety of high-speed aircraft.

The earliest group of supersonic aircraft are all rocket powered and date from the earliest, experimental era of high-speed flight. The Douglas D-558-2 Skyrocket (1948-1956), FIGURE 8, was developed around the same time as the X-2. For transonic flight research, it was fitted with a turbojet engine. For later high-supersonic research, it was modified for air-drop launch and rocket-only propulsion. It was the first manned aircraft to reach Mach 2, which it only did once. Like the X-2, this aircraft had a more conventional configuration with wing mounted ailerons and a T type tail with a discrete rudder and aileron. [3]

FIGURE 8 – D558-II

The next interesting aircraft was the North American X-15 (1959-1968), FIGURE 9, which came a few years after the X-2 program. The X-15 was a high altitude and hypersonic research aircraft. It routinely reached altitudes much higher than 100,000-ft and Mach Numbers greater than 5. Its controls surface layout consisted of a large wedge-shaped vertical tail and a horizontal tail with collective and differential control. A lower ventral tail was included in the initial design, but better stability was encountered with it off. Thus, the control suite for the X-15 comprised a pair of all moving horizontal fins (collective for pitch, differential for roll) and a large, upper surface rudder. [14][15]

FIGURE 9- X-15

Moving on to consider aircraft that takeoff from conventional runways. We next look at the delta wing Lockheed SR 71 (1964-1999), FIGURE 10. It was a high-speed intelligence / surveillance and reconnaissance aircraft with a cruise speed of around Mach 3+. The control surfaces of the SR-71 consist of two all moving vertical fins, then two inboard elevons, and two outboard elevons. [16]

FIGURE 10 – SR-71

The General Dynamics F-111 (1964-1998), FIGURE 11, was a supersonic, multi-role combat aircraft with a max speed of Mach 2.5. The F-111C had a vertical tail with rudder for lateral directional control and an all moving horizontal tail (collective for pitch and differential for roll). Wing mounted flaps were used for takeoff and landing lift enhancements only. [17]

FIGURE 11 – F-111

From these vehicles, we see few common traits. The first of which is that these vehicles all have substantial vertical tail volumes to ensure positive static directional stability; ($dCn/d\beta$ >0). As discussed in Section II, while positive static directional stability is not an essential requirement to make for an inherently stable Dutch Roll mode ($Cn\beta dynamic$ >0) it may prove essential to make for a controllable vehicle so that *LCDP*>0. Post D558 and X-2, we also see the common use of all-moving "tailerons" and inboad/outboard "elevons" usable under a complex control mix scheduling scheme.

V. Could the X-2 be Salvaged with a Change in Control Laws? Or Does It Need to be Aerodynamically Reconfigured?

In this section, we ask and answer if the overall shape of the X-2 could have been maintained, but flying qualities improved with changes to the control system? Or was the X-2 in need of a major configuration change?

We examine three options here: 1) to enlarge the vertical tail/rudder, 2) to create a Mach and α scheduled Aileron-Rudder Interconnect (ARI), and/or 3) to implement differential horizontal tail control for roll.

First, we consider the larger vertical tail/rudder. For the larger vertical tail analysis, we scale the dimensions of the baseline tail upwards by 30% (i.e 30% more tip and root chord as well as 30% greater exposed height). FIGURE 12 shows a comparison between the orignal vertical tail and rudder versus the scaled up version. In Section V, we will see that the vertical tail size grows, we see that the gain in $dCn/d\beta$ improves both lateral-directional stability ($C_n\beta\ dynamic$) and lateral-directional controllability (*LCDP).* We do realize that a pitfall of making the vertical tail larger is its effect on crosswind trim capabilities for landing. In crosswind, the larger tail can have a strong enough weathervane effect to where it saturates the rudder and/or aileron control power depleting any remaining margin for maneuvers. A secondary consideration of an enlarged vertical tail is its associated weight, which will drive the center-of-

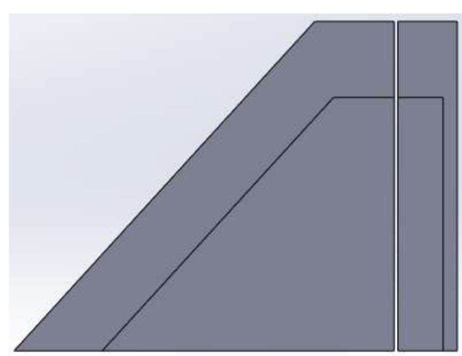

FIGURE 12- Larger Vertical Tail vs Original

gravity further aft or demand nose ballast. For this paper, we assume that mass properties remain constant with an increase in the vertical tail.

We also contemplate improving LCDP by adding a modern flight control system Mach-and-α scheduled aileron-rudder interconnect (ARI) to the X-2. The goal of the ARI is to utilize the primary yaw controller, the physical "rudder," to trim the induced yawing moment of the primary roll controller to zero. A simple ARI can be created using a gain coefficient based on the ratio of the yawing moment of the primary yaw controller to the yawing moment of the adverse yawing source. A mechanical view of an ARI system is shown in FIGURE 18. The ARI for this analysis will treat the ailerons as antisymmetric collective deflections and a set rudder deflection.

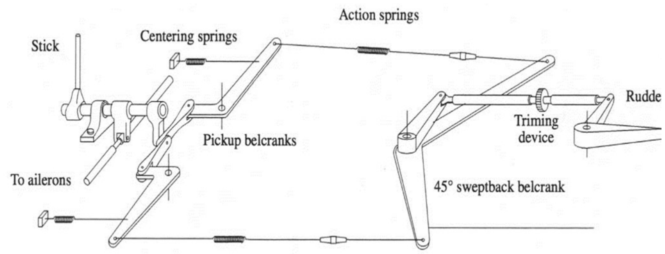

FIGURE 13- Example of a mechanical Aileron Rudder Interconnect System as found on a Fairchild PT-19 [18]

With the prevalence of differential tail control being used on a significant number of high-speed aircraft, this appears to be a potential solution. Differential tail for roll control at high-speeds rather than aileron could help address the severe adverse yaw that the X-2 experienced. Similarly, we can create an alternative ARI utilizing the rudder and the differential tail.

For the next analysis the original aileron and rudder configuration will be compared to a differential tail and rudder configuration. For each case a tentative ARI scheme can be scheduled throughout the flight envelope. This process is completed using pitch trimmed data.

A. Developing the Aerodynamic Database to Screen Aircraft for Handling Qualities Flaws

To create an aerodynamic database for the X-2, we used the potential flow solver VORLAX2022a.[19] VORLAX 2022a is an updated more efficient version of a 1977 FORTRAN program originally written at Lockheed by Luis Miranda under contract for NASA.[20] For use in VORLAX, the aircraft is modeled as a series of flat plates upon which, a grid of vortices can be applied. The key aerodynamic coefficients that are obtained from VORLAX are lift, induced drag, side force, pitching moment, yawing moment, and rolling moment. VORLAX is also capable of estimating the dynamic derivatives of an aircraft as well. This code was chosen for the analysis, as it is useful for rapid database generation while remaining fairly accurate to capture trends. For creation of the panel model detailed dimensions of the aircraft were obtained from NACA RM L57J28a.[21] ; see FIGURE 14.

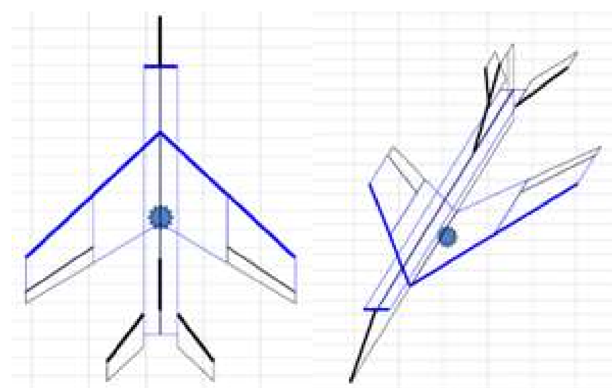

FIGURE 14 - Visualization of VORLAX panel model in top-down view (left) and oblique view (right)

The VORLAX aerodynamic database was generated over a range of Mach Numbers from 0.7 to 2.5 and angles-of-attack from 0-deg to +24-deg. Mass properties about the moment reference point are taken at the aircrafts empty (post-burn) weight: *W*=12,375 lbm, *Ixx*=5,043-slug-ft^2, *Iyy*=25,474-slug-ft^2 and *Izz*=29,106-slug-ft^2.[3]

To obtain a thorough database, a total of 21 cases need to be run in VORLAX. The first seven are to obtain data for the base configuration, aileron deflection, rudder deflection, and the dynamic derivatives. The remaining 14 cases are focused on the deflection of the horizontal tail which is split into two control effector cases. The first case is collective horizontal tail deflection (conventional elevator) and the second is differential deflection (elevon). Seven deflection cases are used to help ensure that interpolation between cases is fairly accurate, as at high-speed and angle of attack, nonlinear effects can be observed. This is done to ensure that the interpolations are good approximations as the yawing and rolling moments are highly dependent on angle of attack, Mach, and elevator deflection. Some of these trends are not linear as well so having multiple steps in deflections help ensure the nonlinearities are captured. The differential tail cases were taken at a 5-degree offset from the respective collective case. A summary of these runs is listed below in TABLE 2 and TABLE 3.

TABLE 2

Case	Aero Dynamic Parameters Obtained
Base (No Control Surface Deflection)	C_L, C_D, C_Y, C_m
Base at 1 deg of Sideslip	$C_L, C_D, C_Y, C_m, \frac{dC_l}{d\beta}, \frac{dC_n}{d\beta}$
Ailerons Deflected 30 deg (No Side Slip)	$\frac{dC_l}{dail}, \frac{dC_n}{dail}$
Rudder Deflected 30 deg (No Side Slip)	$\frac{dC_l}{drud}, \frac{dC_n}{drud}$
Pitch Rate (q) dynamic derivative	C_{mq}
Yaw Rate (r) dynamic derivative	C_{nr}, C_{lr}
Roll Rate (p) dynamic derivative	C_{np}, C_{lp}

TABLE 3

Collective (C_m)	Differential $\left(C_m, \frac{dC_l}{dtail}, \frac{dC_n}{dtail}\right)$	
	Left Surface	Right Surface
+25°	+30°	+20°
+15°	+20°	+10°
+5°	+10°	0°
0°	+5°	-5°
-5°	0°	-10°
-15°	-10°	-20°
-25°	-20°	-30°

B. Basic Controls Neutral Aerodynamic Data with Baseline and Enlarged Vertical Tails

FIGURE 15, shows the lift coefficient as a function of angle-of-attack from VORLAX. As the aircraft's speed increases, the lift curve slope decreases. Note that VORLAX does not capture stall or shock induced separation thus the decline in lift is not captured. To show relative accuracy of VORLAX, FIGURE 16 shows a comparison of Wind Tunnel Data vs VORLAX. [21] From FIGURE 16, we can see that the results are reasonably close, and that the wind tunnel data can potentially be used to bound the lift coefficient if needed.

Another key figure of interest is pitching moment vs lift curve slope shown in FIGURE 17. With the curves upward (negative) slopes, we can see that the X-2 is statically stable in pitch at all Mach numbers. As the Mach number increases, we can see an increase in pitch stability. This is expected as the aerodynamic center moves from the quarter chord to the half chord once the wing is supersonic.

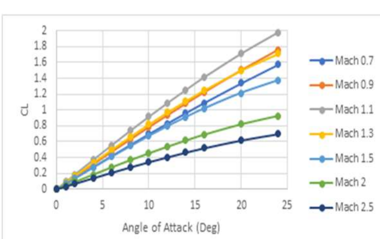

FIGURE 15 - CL vs α from VORLAX

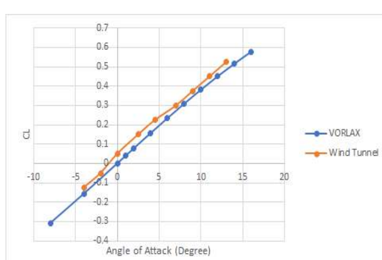

FIGURE 16 - CL vs α Comparison between VORLAX and Tunnel at Mach 2.29

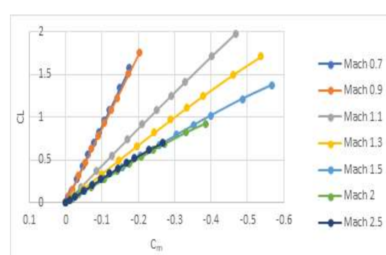

FIGURE 17 – Cm v CL from VORLAX

FIGURE 18 compares the yawing moments vs angle of attack for both the original configuration and the large vertical. Overall, the trends between the two configurations are quite similar but, the larger vertical tail has about a 0.001 improvement in the inherent yaw stability. This trend appears throughout all Mach Numbers where for example at Mach 2.5 the original configuration has a value of around 0.003 compared to 0.004 for the larger vertical and at Mach 0.9 the original has a value of 0.006 vs 0.007 for the larger vertical. From this we can see that as the Mach number increases the yaw stability of the aircraft decreases. For all Mach Numbers, we show that the X-2 is statically stable in yaw.

FIGURE 19 shows the inherent rolling moment vs angle of attack for both the original configuration and the large vertical. In both cases, the dihedral effect increases with increasing angle of attack but also decreases with increasing Mach Number. With the large vertical, the dihedral effect decreases slightly at each angle of attack and Mach number leading to slightly reduced roll stability. With the rolling moment curve negative for all cases, we conclude that the X-2 was stable in roll for stick-fixed condition.

With the increase in inherent yawing moment stability and decrease in rolling moment stability, there is a significant effect on the lateral directional stability of the aircraft as Cn Beta Dynamic and LCDP are dependent on these parameters.

FIGURE 20 shows the effect of the large vertical on $Cn\beta dynamic$. The values were trimmed on this plot to show the effect at smaller angles of attack as this is where the border of the Skow Criterion occurs. [8] As the angle of attack increases, *CnβDynamic* continues to increase and thus is really only a major concern at angles of attack less than 15-deg. It is shown that increasing the vertical tail results in a substantial jump in *CnβDynamic*. For the original configuration at Mach 2.5, the Skow criterion was not satisfied until around 8-deg whereas the large vertical configuration is satisfied at only 5-deg. [8] Additionally for the large vertical tail configuration, for Mach 1.1 to 1.5, the Skow criterion is met for all positive angles of attack. This indicates that the X-2 could have possibly been a good aircraft to fly just past the supersonic boundary.

The other key parameter to examine is LCDP shown in FIGURE 21, overleaf. Overall, the trends between the original and large vertical configuration are the same with the only difference being the magnitude. The large vertical has significantly high LCDP values with them being around 0.002 higher. From the Bihrle-Weismann plot, we know that LCDP must be positive thus the larger vertical also helps ensure the aircraft is firmly in region A. For the original configuration at Mach 2-2.5, it can be seen that the aircraft will depart from stable flight at around 15-deg whereas with the larger vertical, departure begins to occur around 22-deg. This is a massive

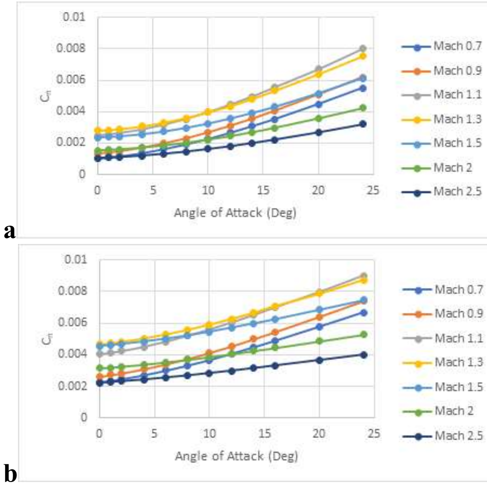

a
b

FIGURE 18- $dC_n/d\beta$ vs α
(Top Original, Bottom Large Vertical)

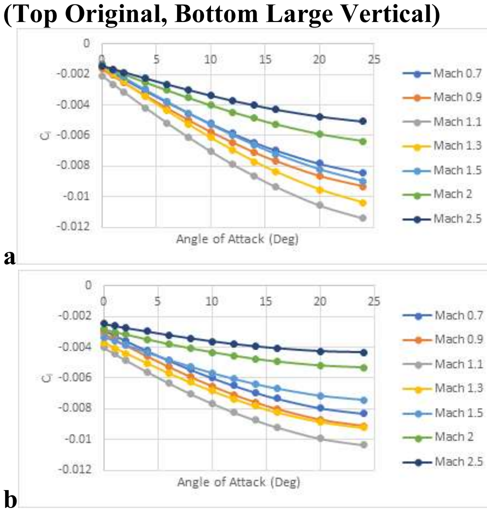

a
b

FIGURE 19- $dC_l/d\beta$ vs α
(Top Original, Bottom Large Vertical)

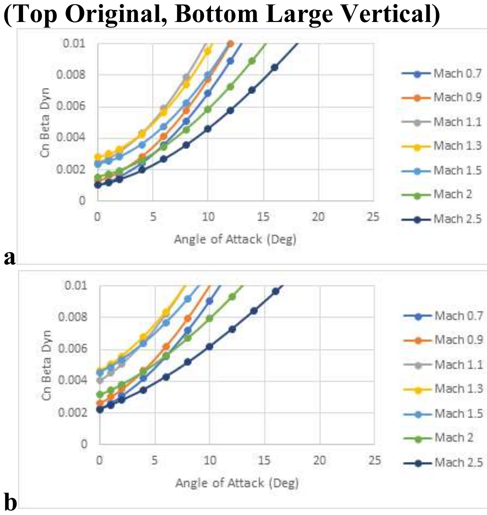

a
b

FIGURE 20 - CnβDynamic vs α
(Top Original, Bottom Large Vertical)

improvement in lateral directional stability if a maneuver is to occur at high speeds. When the aircraft is simply only performing supersonic cruise the effects of the increased LCDP will be felt much less.

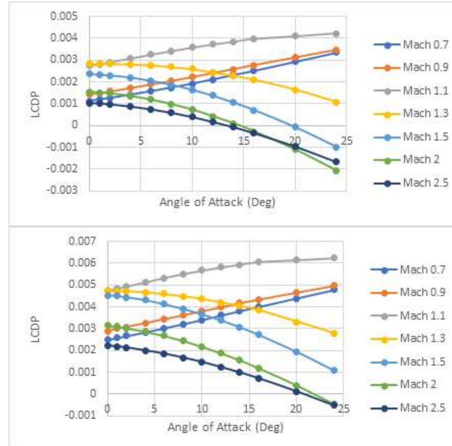

FIGURE 21- LCDP vs α
(Top Original, Bottom Large Vertical)

C. Secondary Processing of the Aerodynamic Database

For the creation of Mach/Altitude "Sky Maps," the data must first be massaged through a series of transformations. To assist in checking stability at a variety of center of gravity points, a moment transformation is first done based on the moment reference point of the data. The reference VORLAX data is in Stability Axis, so it first must be transformed into Body Axis so that the moment transformation can be computed. [22] The new Body Axis data is saved to a sheet and then converted back to into Stability Axis. Another additional layer was added to trim the data to a zero-pitching moment condition. This helps elementarily address the point of while an aircraft maybe ultimately be stable it may not be able to be trimmed. Using the various control surface deflection cases, an elevator deflection can be obtained that corresponds to zero pitching moment. For the cases where a larger elevator deflection is required the data is blanked.

Static stability will not be discussed in detail, for more details on the process and verification refer to [2]. This section will focus on the resulting Sky Maps from the analysis and the conclusions drawn from them.

D. Longitudinal Stability for Original Configuration

The first area of interest is the longitudinal dynamic stability. The key screening parameters in this area of focus are the Short Period and the Short Period damping ratio.

A key concern of the Short Period frequency is that if it becomes too high, there is the possibility that it will sit on top of one of the rigid body structural natural frequencies. If this occurs, then resonance may occur causing violent vibrations shaking the plane apart.

From FIGURE 22, we can see that flying supersonic at low altitude and high-speed excites the Short Period frequency to levels of concern. This results in high-speed flight being restricted to mainly modest to higher altitudes (>40,000 ft).

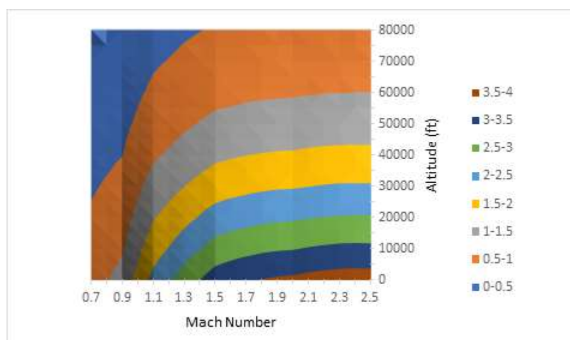

FIGURE 22 – Short Period Sky Map

As the altitude increases and speed increases, we can see in FIGURE 23 that the damping begins to fall off drastically. A modest 20% damping ratio is achieved for only a small band of lower altitude and supersonic flight. This then begs the question, how does one balance these two parameters? To keep the damping good, the pilot must fly the aircraft at relatively lower altitudes and high speeds. This is not ideal and would result in an unrealistic restriction on the flight envelope. To solve this problem, synthetic damping will likely need to be added to the aircraft via a closed loop control system.

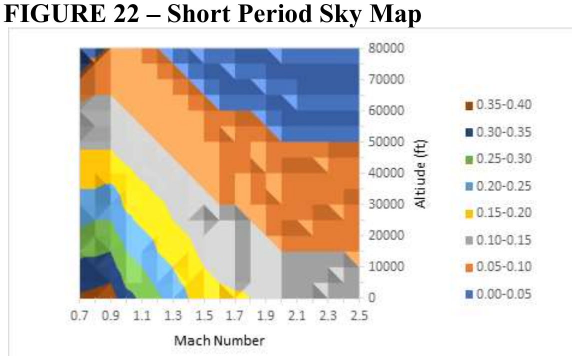

FIGURE 23 – Short Period Damping Sky Map

FIGURE 24 plots the pitch responsiveness and Short Period frequency on a Sky Map derived from the Category A chart from MIL 8785-C. [9] Level 1 characteristic are filled green, Level 2 characteristic are yellow, and Level 3 characteristic are red. From this figure we can see that the X-2 has overall okay longitudinal stability over the entire flight envelope. Some discrepancies in the center of gravity location may be the cause the deceased performance shown here.

E. Bihrle-Weissman and Lateral-Directional Stability for Original Configuration

For lateral directional stability there are significantly more key parameters of interest: Dutch Roll Frequency and damping, the Roll and Spiral time constants, $C_n\beta\ dynamic$ and $LCDP$.

When looking at the Dutch Roll frequency one must ensure that the frequency is not too slow or too fast. MIL8785C suggests a minimum frequency of 0.4-1 rad/s (0.06-0.16 Hz). From FIGURE 25, we see that the Dutch Roll frequencies are reasonable throughout the flight envelope. At low altitude and high-speed, again the frequency does get quite fast where coupling may occur. The Dutch Roll damping shown in FIGURE 26, appears to be highly dominated by altitude with speed having very little influence. Overall, the damping is quite lightly damped and will likely need synthetic damping to improve the handling qualities. This can be achieved by wiggling the rudder or other yaw device through the implementation of a yaw damper system.

$LCDP$ is shown in FIGURE 27. An interesting trend that can be observed is that $LCDP$ appears to be a strong function of speed with altitude having very little effect. As the speed increases $LCDP$ decreases greatly going to smaller values pushing the aircraft toward the F-region or other non-spin resistant regions on the Weismann chart. For A-Region characteristic, $LCDP$ must be positive. As the value gets closer to zero, the lateral-directional handling characteristics of the aircraft being to suffer.

$C_n\beta\ dynamic$ is shown in FIGURE 28, overlap. From this figure we see that $C_n\beta\ dynamic$ is a strong of function of both altitude and speed. We can see that for a large portion of the flight envelope, $C_n\beta\ dynamic$ does not meet the Skow criterion, anything under the orange curve. [8] For an aircraft to be in the A-Region, $C_n\beta\ dynamic$ should be greater than 0.004. This is where the X-2 suffers as most of the flight envelop that it operated in was where $C_n\beta\ dynamic$ was low. This is the key parameter that results in the X-2 having poor lateral-directional stability.

Altitude (ft)	Mach 0.7	0.8	0.9	1.0	1.1	1.2	1.3	1.4	1.5	1.6	1.7	1.8	1.9	2.0	2.1	2.2	2.3	2.4	2.5
80000			2	2	2	2	2	2	2	2	2	2	2	2	2	2	2	2	2
75000		2	2	2	2	2	2	2	2	2	2	2	2	2	2	2	2	2	2
70000	2	2	2	2	2	2	2	2	2	2	2	2	2	2	2	2	2	2	2
65000	2	2	2	2	2	2	2	2	2	2	2	2	2	2	2	2	2	2	2
60000	2	2	2	2	2	2	2	2	2	2	2	2	2	2	2	2	2	1	1
55000	2	2	2	2	2	2	2	2	2	1	1	1	1	1	1	1	1	1	1
50000	2	2	2	2	2	2	2	1	1	1	1	1	1	1	1	1	1	1	1
45000	2	2	2	2	2	2	1	1	1	1	1	1	1	1	1	1	1	1	1
40000	2	2	2	2	2	1	1	1	1	1	1	1	1	1	1	1	1	1	1
35000	2	2	2	2	1	1	1	1	1	1	1	1	1	1	1	1	1	1	1
30000	2	2	2	2	1	1	1	1	1	1	1	1	1	1	1	1	1	1	1
25000	2	2	2	1	1	1	1	1	1	1	1	1	1	1	1	1	1	1	1
20000	2	2	2	1	1	1	1	1	1	1	1	1	1	1	1	1	1	1	1
15000	2	2	2	1	1	1	1	1	1	1	1	1	1	1	1	1	1	1	1
10000	2	2	2	1	1	1	1	1	1	1	1	1	1	1	1	1	1	1	1
5000	2	2	1	1	1	1	1	1	1	1	1	1	1	1	1	1	1	1	1
0	2	2	1	1	1	1	1	1	1	1	1	1	1	1	1	1	1	1	1

FIGURE 24- MIL 8785C Levels for Category A Flight

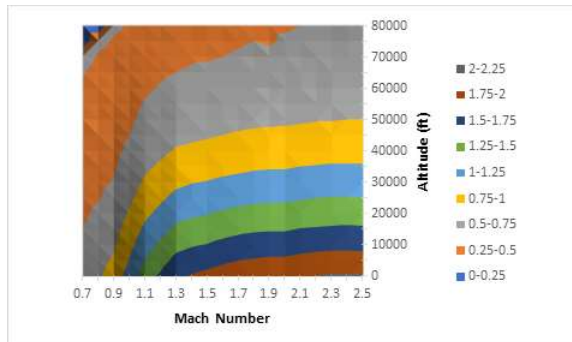

FIGURE 25 – Dutch Roll Sky Map

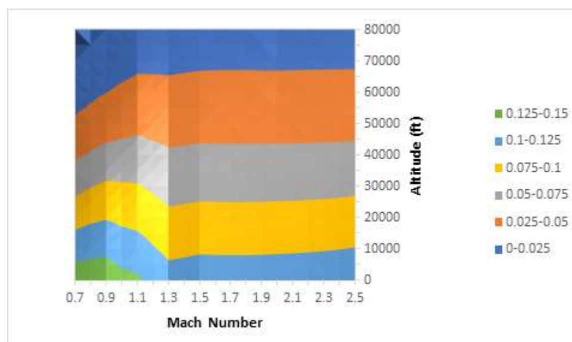

FIGURE 26 – Dutch Roll Damping Sky Map

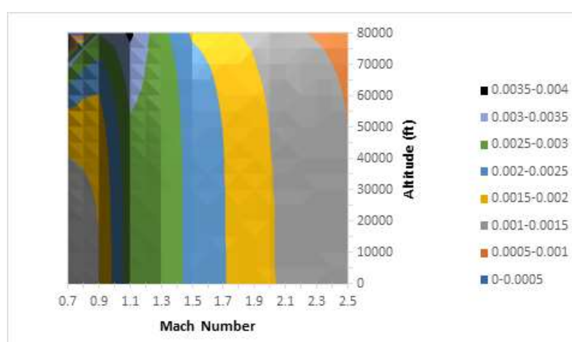

FIGURE 27- LCDP Aileron

The next parameters to examine are the Roll and Spiral modes. When these frequencies lie on top of each other, there may be a chance that “Lateral Phugoid” coupling may occur. [6] Teodorescu noted the existence of this previously neglected lateral-directional oscillatory-departure mechanism generated by the Roll time constant of any lateral control input exciting the Spiral mode. This mode is extremely difficult to suppress. [7]

The Spiral mode is shown in FIGURE 29. An interesting trend to observe is that at subsonic to transonic speeds there is strong dependence on speed. Once the aircraft is supersonic, it appears that the Spiral mode is mainly a function of altitude. Once at supersonic speeds, the Spiral Mode time constant only increases ever so slightly.

The Roll mode is shown in FIGURE 30. We observe a similar trend to the Spiral mode: at subsonic to transonic speeds, there is a strong dependence on altitude and speed. Once supersonic, the Roll mode appears to only dependent on altitude and approach a steady state value only.

When looking at the magnitudes of the Spiral mode and Roll mode it can be determined that the Spiral mode is significantly greater than the Roll mode and thus Roll-Spiral “Lateral-Phugoid” coupling will likely never occur for the X-2.

F. Flight Envelope Limitations due to Trim and Stability and controllability restrictions

To gain more insightful details on suitable flight envelopes for an aircraft, the presented sky maps can be further refined. There are numerous ways to restrict the data based on what the designer is focused on. If the aircraft is suspected to be prone to inertia coupling, a potential solution is to take the percent difference between the Short Period and Dutch Roll frequencies as shown in FIGURE 31. This allows the engineer to see where in the flight envelope the frequencies lie on top of each other. When the two frequencies are close there is potential cross talk between the two and that can feed into inertial coupling. A similar idea can be applied to the Roll and Spiral modes to try and restrict coupling between those two modes.

As discussed previously, a simple restriction on $C_n\beta\ dynamic$ should come from the Skow Criterion. [8] This is shown in FIGURE 32, overleaf. This allows the designer to quickly see where in the flight envelope lateral directional stability is lacking or if those regions can be avoided.

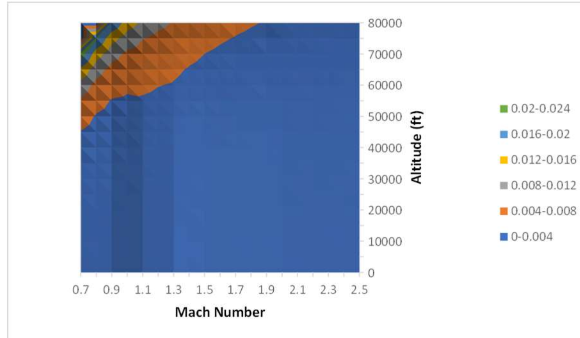

FIGURE 28- $C_n\beta\ dynamic$ Aileron

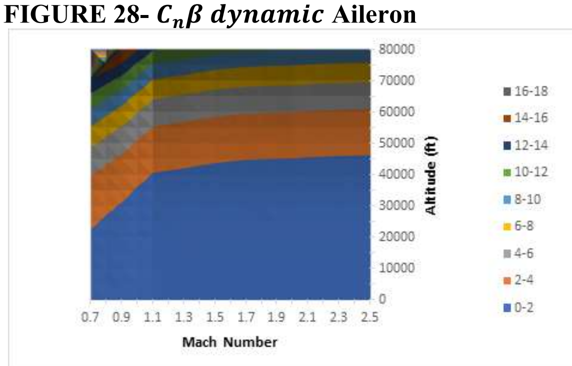

FIGURE 29- Spiral Mode Time Constant

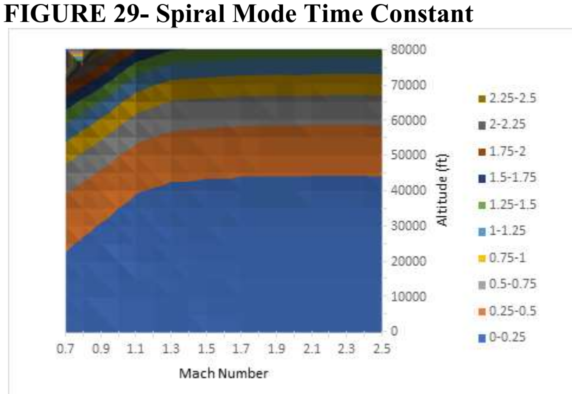

FIGURE 30- Roll Mode Time Constant

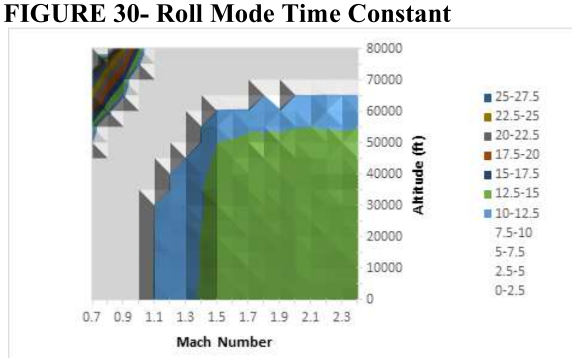

FIGURE 31 – Checking Percent Difference Between Short Period and Dutch Roll Modes (within 10%)

When targeting ideal values for certain parameters the flight envelope may become entirely blanked out as the various screening parameters are restricting different parts of the envelope. This is easily seen in FIGUREs 31 and 32 where, if the two plots were superimposed the only desirable region is the top left corner of the envelope. As more and more restrictions are placed on the aircraft the more difficult it becomes to find a suitable flight envelope. This is seen in those two figures as high-speed flight is totally inaccessible if those two criteria need to be met. This results in the engineer having to decide which of the stability screening parameters are going to bound the problem.

G. Assessment of the impact of Aileron-Rudder Interconnect

To address the adverse yaw problems, a simple ARI scheme can be plotted as a function of Mach and altitude. Using a simple gain ratio will allow for an overall magnitude of effectiveness and feasibility to be determined. More complex control schemes could be investigated that make use of state-space analysis. These more rigorous/complex methods would allow for unsymmetric-differential tail or aileron, potentially opening more feasible solutions.

For the conventional X-2 configuration, the ARI scheme shown in FIGURE 33 was obtained. There are a couple of interesting trends to notice. First, is that up until around Mach 1.4 the ARI gains are positive until switching sign and becoming more negative at higher altitudes. For a majority of the high-speed flight and high altitude, a gain of around -0.1 is required. When first plotting the ARI obtained when using the differential tail as the primary roll controller, it was noticed that all gains were essentially zero. With the differential tail having no values of interest, it is not included here.

However once considering the sideslip angle (Beta) that can be trimmed, the ineffective differential tail control makes sense. FIGURE 34 shows the sideslip angles that the conventional aileron configuration can trim per degree of control surface deflection. At subsonic speed the sideslip trim is quite high but decreases with increasing Mach number. It should be noted that not all angles of attack are included with the higher Mach number cases as the aircraft could not trim to zero pitching moment at those points. Assuming 30-deg of deflection out of the rudder and ailerons, only 0.33-deg sideslip per degree of control surface deflection is required to trim to 10-deg of sideslip. At subsonic and small angles of attack, the *X-2* can trim to around β=+/-40-degr. Even at the highest

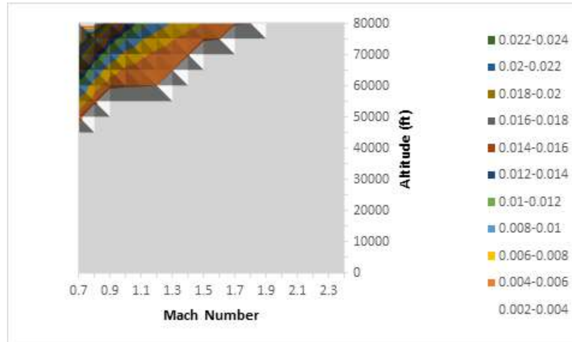

FIGURE 32 – Available Flight Envelope if bounded Skow Criterion

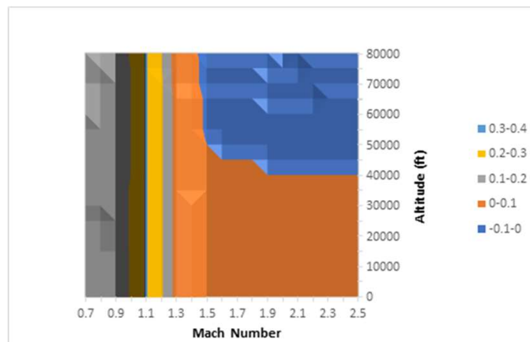

FIGURE 33 – ARI Scheduling Required when using Aileron for Roll Control

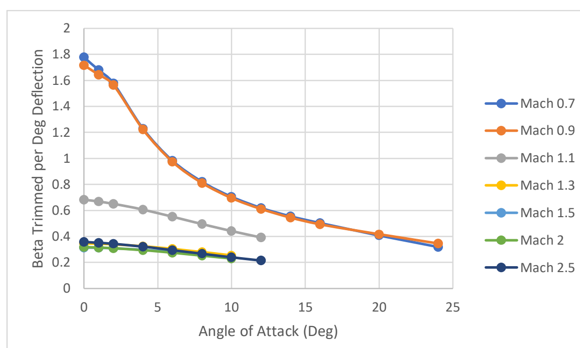

FIGURE 34- Aileron Sideslip to Trim

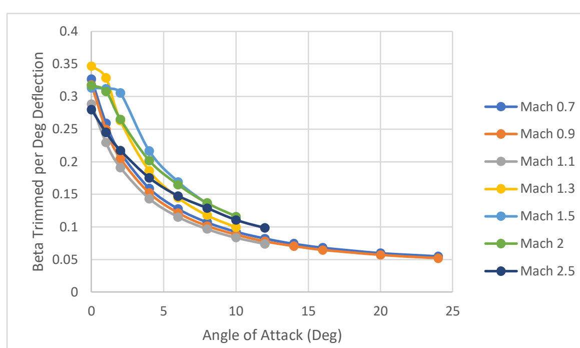

FIGURE 35- Differential Tail Sideslip to Trim

Mach Number run, the conventional configuration can trim to about 8-degrees of sideslip.

FIGURE 35 shows the sideslip angles that the differential tail configuration can trim to. From the figure it is concluded that no roll control can be established from the differential horizontal tail, as realistically not even a degree of sideslip is trimmable. At 0-deg angle of attack, around a maximum of 10-deg of sideslip can be achieved, with increasing angle of attack rapidly decreasing sideslip performance. At around 5-deg angle of attack, the sideslip is around 3-deg. In addition, using a differential tail requires some level of collective deflection for trim thus, a full 30-deg of elevator deflection is not obtainable like the aileron case. This indicates that the horizontal tail is just too small to be effective. While differential all moving horizontal tails appear to be effective on many modern high-speed aircraft, it does not work on the *X-2* due to its small size.

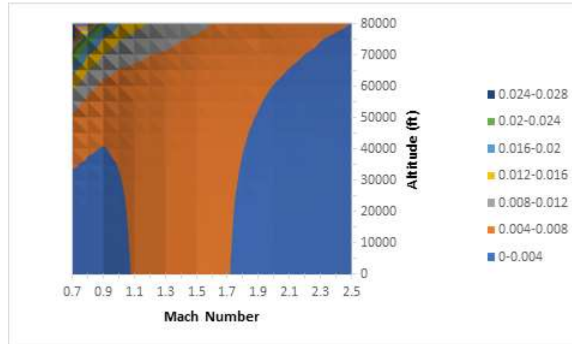

FIGURE 36: $C_n\beta$ *dynamic* of X-2 with Large Tail

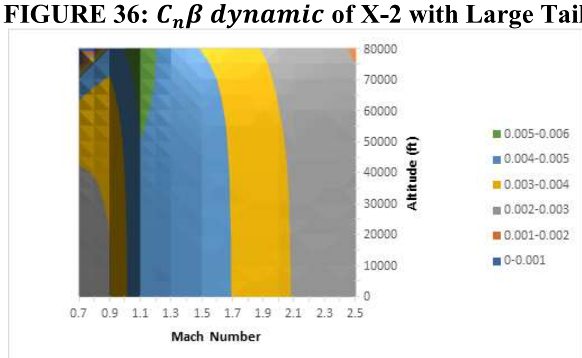

FIGURE 37- LCDP of X-2 with Larger Vertical Tail

H. Assessment of the impact of the enlarged Vertical Tail

Now looking at the impact on the lateral-directional stability of the X-2 run with a larger vertical tail. With the bigger tail, the X-2 has greatly increased lateral directional stability.

When comparing large tail configuration $C_n\beta$ *dynamic* shown in FIGURE 36, to the original configuration bounded by Skow Criterion back in FIGURE 32, we can see that a much larger portion of the flight envelope has opened. The overall maximum value of $C_n\beta$ *dynamic* increased from 0.024 to 0.028. We can now see that a desirable pocket in the middle of the flight envelope has now open up were the X-2 should now be spin resistant. Remember on the updated Bihrle-Weissman chart, *LCDP* needs to be positive and $C_n\beta$ *dynamic* greater than 0.004.

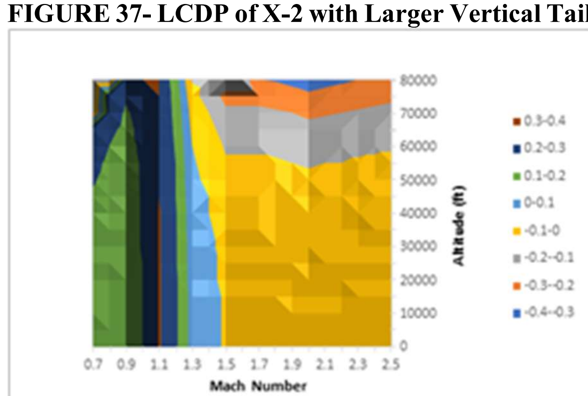

FIGURE 38-ARI Scheduling Required when using Aileron for Roll Control

When looking at *LCDP* shown in FIGURE 37, there are no major differences in the trends first observed in FIGURE 27. The magnitude of *LCDP* did increase by 0.002, with more of the flight envelope falling in between the values of 0.005 and 0.002 when compared to the base configuration.

The last parameter of interest to compare is the ARI gains. When comparing FIGURE 38 to FIGURE 33, we can see that the gains have been increased slightly. For the large tail configured X-2, if an ARI was utilized it appears that on average the ARI gains would have to have a 10% margin added on when flying supersonic at high altitudes. Additionally, when above Mach 1.4, now the gains are negative at all altitudes.

While increasing the tail has seemed to greatly increase the lateral-directional stability one must also keep in mind the mass properties of the aircraft. With the mass properties held constant as discussed in Section V the feasibility of actually extending the tail to be this large is likely not possible. For this reason, other key parameters like the Dutch Roll Frequency and damping will not be addressed.

VI. Summary & Conclusion

In this paper we show a variety of stability and control screening parameters that identify the basic handling of an aircraft. The key parameters of interest are: Short Period frequency and damping, Dutch Roll frequency and damping, $LCDP$, $C_n\beta\ dynamic$, the Roll mode, and the Spiral mode.

When looking that the longitudinal stability of the X-2, it can be determined that throughout the typical flight envelope the aircraft had a reasonable Short Period frequency with the damping being quite light. When plotting the handling qualities, we found that the X-2 had Level 1 and Level 2 regions in the flight envelope resulting in satisfactory handling qualities.

For lateral directional stability, the X-2 suffered greatly from $C_n\beta\ dynamic$. For the original configuration, only a small region of low speed and high-altitude flight met the Skow criterion. With the larger vertical tail configuration, a much larger flight envelope offers favorable stability & control. With the larger vertical tail, the Dutch Roll frequency and $LCDP$ were satisfactory even without ARI. At the same time, we noted that there are substantial areas where the Short Period and Dutch Roll frequencies are within 10% of each other. Given its mass properties, concerns that Inertia Coupling can develop within the flown flight envelope were shown. With baseline or enlarged vertical tails, we found that the X-2 did not suffer from an unstable Roll Mode or Spiral Mode or a coupling of the two modes.

From this analysis, we can offer some conclusions for general high-speed vehicle design. For the lateral-directional stability criteria to be satisfied, high-speed aircraft really require larger than expected vertical tails. The larger vertical tails help shift $C_n\beta\ dynamic$ to be greater than the Skow Criterion to ensure that the aircraft is departure resistant. As these vehicles fly faster, the damping on the frequencies become quite poor thus, synthetic damping and some type of control system is likely a necessity. The last point of concern is that as these aircraft fly faster and especially at lower altitudes, the aerodynamic frequencies become so large resulting in the possibility of exciting the structural frequencies causing vibrations or Inertia Coupling.

Acknowledgments

We would like to that Professor Ramana Grandhi at the Air Force Institute of Technology for enabling this collaborative effort to develop tools to assess the configurations of future high-speed aircraft. This research was supported, in part, by an appointment to the Student Research Participation Program at the U.S. Air Force Institute of Technology, administered by the Oak Ridge Institute for Science and Education through an interagency agreement between the U.S. Department of Energy and AFIT.

References

[1] Whitford, Ray, "Lessons Learned from the Bell X-2 Program," SAE Transaction, Vol. 105. Section: Journal of Aerospace. Pp. 1407-1421, 1997, https://www.jstor.org/stable/44650531

[2] O'Brien, K.P. and Takahashi, T.T., "An Investigation of the Bell X-2 and the Factors that Led to Its Fatal Accident," AIAA 2022-3203, 2022.

[3] Day, R.E. "Coupling Dynamics in Aircraft Design: A Historical Perspective," NASA SP-532, 1997.

[4] Takahashi, T.T., Aircraft Performance & Sizing, Vol. II: Applied Aerodynamic Design, Momentum Press, New York, NY, 2016. 276 pages. ISBN-13: 978-1606509456

[5] Yechout, T.R., Introduction to Aircraft Flight Mechanics, Second Edition, AIAA, 2014.

[6] Takahashi, T.T., Griffin, J.A. and Grandhi, R.V., "A Review of High-Speed Aircraft Stability and Control Challenges," AIAA 2023-3231, 2023.

[7] Teodorescu, B.C., "Lateral Directional Oscillatory Departure Criteria for High Angle-of-attack Flight Conditions," U.P.B. Sci. Bull., Series D, Vol. 68, No. 3, 2006.

[8] Skow, A.M. and Titiriga, A., "A Survey of Analytical and Experimental Techniques to Predict Aircraft Dynamic Characteristics at High Angles of Attack," AGARD CP-235, 1978.

[9] MIL STD-8785C, Flying Qualities of Piloted Airplanes, U.S. Department of Defense, Washington, D.C., November 5,1980.

[10] Chambers, J.R. and Anglin, E.L., "Analysis of Lateral-Directional Stability Characteristics of a Twin-Jet Fighter Airplane at High Angles of Attack," NASA TN D-5361, 1969.

[11] Mason, W.H., "High Alpha and Handling Qualities Aerodynamics," Configuration Aerodynamics Class Notes from Virginia Tech 2018, see: http://www.dept.aoe.vt.edu/~mason/Mason_f/HiAlphaBasicsPres.pdf (accessed November 5, 2021)
[12] Weissman, R., "Status of Design Criteria for Predicting Departure Characteristics and Spin Susceptibility," AIAA 74-791, 1974.
[13] Weissman. R., "Preliminary Criteria for Predicting Departure Characteristics' Spin Susceptibility of Fighter-Type Aircraft," AIAA Journal of Aircraft, Vol. 10, No. 4, April 1973.
[14] Hallion, Richard, "On the Frontier Flight Research at Dryden 1946-1981" NASA SP 4303, 1984
[15] Griffin, J.A. and Takahashi, T.T., "Aero-Spaceplane Mission Performance Estimations Incorporating Atmospheric Control Limits," AIAA 2022-3656, 2022.
[16] Gibbs, Yvonne, "NASA Armstrong Fact Sheet: SR-71 Blackbird," NASA.gov. Last Updated August 7, 2017, *See:* https://www.nasa.gov/centers/armstrong/news/FactSheets/FS-030-DFRC.html
[17] Gibbens, P.W., "Manoeuvre Controller Design for an F-11C Flight Dynamics Model," Air Operation Division Aeronautical and Maritime Research Laboratory, DSTO-RR-0129.
[18] "Chapter 17 A Couple of Bloopers!", JOURNEY IN AERONAUTICAL RESEARCH: A Career at NASA Langley Research Center, Monographs in Aerospace History, Number 12. history.nasa.gov, *See:* https://history.nasa.gov/monograph12/ch17.htm
[19] Souders, T.J. and Takahashi, T.T., "VORLAX 2020: Making a Potential Flow Solver Great Again," AIAA 2021-2458, 2021.
[20] Miranda, L.R., Baker, R.D., and Elliot, W.M., "A Generalized Vortex Lattice Method for Subsonic and Supersonic Flow," NASA CR 2875, 1977.
[21] Fournier, R.H. and Silvers, H.N. "Investigation of the Static Lateral Stability and Aileron Characteristics of a 0.067-Scale Model of the Bell X-2 Airplane at Mach Numbers 0f 2.29,2.78,3.22 and 3.71," NACA RM L57J28a, 1958.
[22] Alexander, M.G., "Subsonic Wind Tunnel Testing Handbook," Wright Laboratory, WL_TR-91-3073, May 1991.